Chemical Engineering Journal 165 (2010) 649–657

Contents lists available at ScienceDirect

Chemical Engineering Journal

journal homepage: www.elsevier.com/locate/cej

Steam reforming of ethanol for hydrogen production: Thermodynamic analysis including different carbon deposits representation

F. Díaz Alvarado, F. Gracia*

Departamento de Ingeniería Química y Biotecnología, Facultad de Ciencias Físicas y Matemáticas, Universidad de Chile, Av. Tupper 2069, 2do Piso, Laboratorio de Catálisis y Energía Combustible, 8370451 Santiago, Chile

ARTICLE INFO

Article history:
Received 14 May 2010
Received in revised form 18 August 2010
Accepted 10 September 2010

Keywords:
Hydrogen
Steam reforming
Ethanol
Thermodynamics
Carbon deposits

ABSTRACT

The importance of H_2 production as an energy carrier in the future has driven the attention to reforming systems, such as steam reforming, partial oxidation or oxidative steam reforming of ethanol, considering thermodynamic and kinetic aspects.

Thermodynamics predicts the equilibrium composition of reactants and products at different temperatures. Previous works represent carbon deposition only as graphite formation, because graphite is present in thermodynamic databases and its properties are known. This work aims to describing equilibrium composition for Reforming systems, including carbon deposits represented as graphite, nanotubes and amorphous carbon.

The obtained results show formation of carbon species below a steam/ethanol ratio equal to 4.0. This region is divided by the dominance of graphite, below 400 °C; and nanotubes, above 400 °C.

Our results indicate that the disappearance of carbon deposits as oxygen/ethanol ratio increses is mainly due to nanotubes removal from equilibrium composition, rather than graphitic species disappearance.

No amorphous carbon was obtained in equilibrium calculations thus, considering the experimental data found in the literature, formation in real systems should be described differently from pure C species.

1. Introduction

The technology of fuel cells and the use of H_2 are proposed as one of the most promising environmental solution in relation to reducing the emission levels in a growing automotive and industrial park, in addition to being more energy efficient than diesel or internal combustion engines [1].

While oil, natural gas and liquefied gas are the main current sources of hydrogen, ethanol has attracted some attention in recent years [2–5]. Ethanol is a renewable resource, easy to store and manipulate, and can be transported safely due to its low toxicity and volatility compared with methanol, the first alcohol used to generate H_2. Moreover, the chemical storage in liquid is considered a good option for hydrogen transport [6].

H_2-production from bioethanol is attractive given the fact that bioethanol is the world most available biofuel, which therefore would allow a renewable production of hydrogen: ethanol can be produced from biomass (such as energy crops and forestry, agricultural or municipal waste), receiving also the name of *bioethanol*. The CO_2 produced during the generation of bioethanol based H_2 is partially reabsorbed from the atmosphere in the growth of biomass, completing a carbon balance near to closed, depending on the considered biomass and its processing [7]. Based on life cycle assessment, the current bioethanol technologies, especially from corn and sugar cane, have been proposed to produce greenhouse gases emissions of the same order of magnitude than those from gasoline technologies [7–9]. However, carbon emissions for bioethanol are lower than gasoline emissions, and bioethanol production also requires less petroleum. Bioethanol generation from cellulose or waste would decrease both parameters [7].

The main reasons for obtaining H_2 from bioethanol, instead of using bioethanol as fuel directly, lie essentially on dealing with the dilution of ethanol during direct utilization [10] (13 mol H_2O/mol C_2H_5OH, approx.) [11]. Furthermore, the bioethanol production may generate other compounds difficult to separate, not desirable in a combustion process. All this implies that it is not advisable to use bioethanol directly in internal combustion engines [10].

* Corresponding author. Tel.: +56 2 9784284; fax: +56 2 6991084.
E-mail addresses: fdiaz.ing@gmail.com (F. Díaz Alvarado), fgracia@ing.uchile.cl (F. Gracia).

1385-8947/$ – see front matter © 2010 Elsevier B.V. All rights reserved.
doi:10.1016/j.cej.2010.09.051

H_2 from ethanol has three main ways for being produced, all expressed as total conversion equations [12,13]:

- Steam Reforming (SR):

$$C_2H_5OH(l)+3H_2O(l) \rightarrow 2CO_2(g)+6H_2(g),\ \Delta H^\circ = 347.5\,[kJ/mol] \quad (1)$$

- Partial Oxidation (POX):

$$C_2H_5OH(l)+1.5O_2(g) \rightarrow 2CO_2(g)+3H_2(g),\ \Delta H^\circ = -510.0\,[kJ/mol] \quad (2)$$

- Oxidative steam reforming (OSR):

$$C_2H_5OH(l)+(3-2x)H_2O(l)+xO_2(g) \rightarrow 2CO_2(g)+(6-2x)H_2(g),$$
$$\Delta H^\circ = 2*(-393.5)-1*(-277.0)-(3-2x)*(-285.8)\,[kJ/mol] = 347.5-571.7x\,[kJ/mol] \quad (3)$$

where x is the molar O_2/C_2H_5OH ratio, abbreviated as O/E ratio. H_2O/C_2H_5OH ratio is abbreviated as S/E ratio (steam to ethanol).

A particular case of reaction (3), commonly used, is [14]:

$$C_2H_5OH(l)+2H_2O(l)+0.5O_2(g) \rightarrow 2CO_2(g)+5H_2(g),\ \Delta H^\circ = 61.6\,[kJ/mol] \quad (4)$$

However, in the OSR system, endothermic or exothermic conditions could be tuned by adjusting the O/E ratio in Eq. (3). Thus, attending global thermodynamic, the system is energetically neutral if:

$$x = 0.61 \Rightarrow \Delta H^\circ = 0\,[kJ/mol] \quad (5)$$

The operation at this point is called autothermal reforming (ATR) [15].

On the reaction mechanism, it is proposed that ethanol is initially converted to ethylene (C_2H_4) or acetaldehyde (CH_3CHO), the first of which is identified as the main precursor for coke formation on the catalyst surface [10,16]. Several papers have been published on hydrogen production from ethanol [10,12,14,17–27], studying mainly metal catalysts. Good yields have been obtained, but the problem of catalyst deactivation due to carbon deposits formation remains open [20,28,16].

In relation to the equilibrium output composition, a thermodynamic analysis by Gibbs free energy minimization has been considered [29–33]. Previous contributions are concentrated in the thermodynamic of gaseous species, and those who consider solid deposits formation, represent carbon deposition as graphite formation.

Nanotubes have been photographed in the carbonaceous deposits of catalytic reforming [20,27,34]. The structure of carbon deposits formed in a catalytic process vary with reaction properties, catalyst type and reaction conditions. According to these specifications, in a reaction system, various types of car-

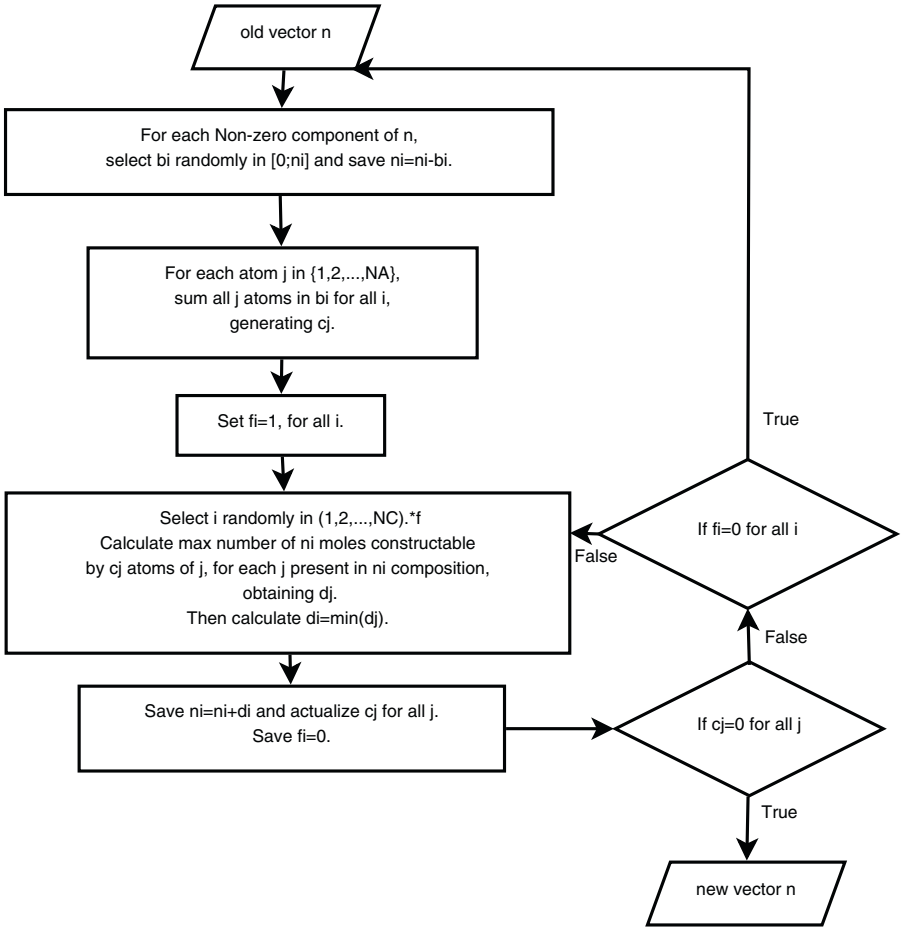

Fig. 1. Flow diagram for composition vector calculation routine. Operator (.*) is a 'component by component' vector multiplication (generates a new vector). [ ] values $\in \mathbb{R}$, instead { } values $\in \mathbb{N}$.

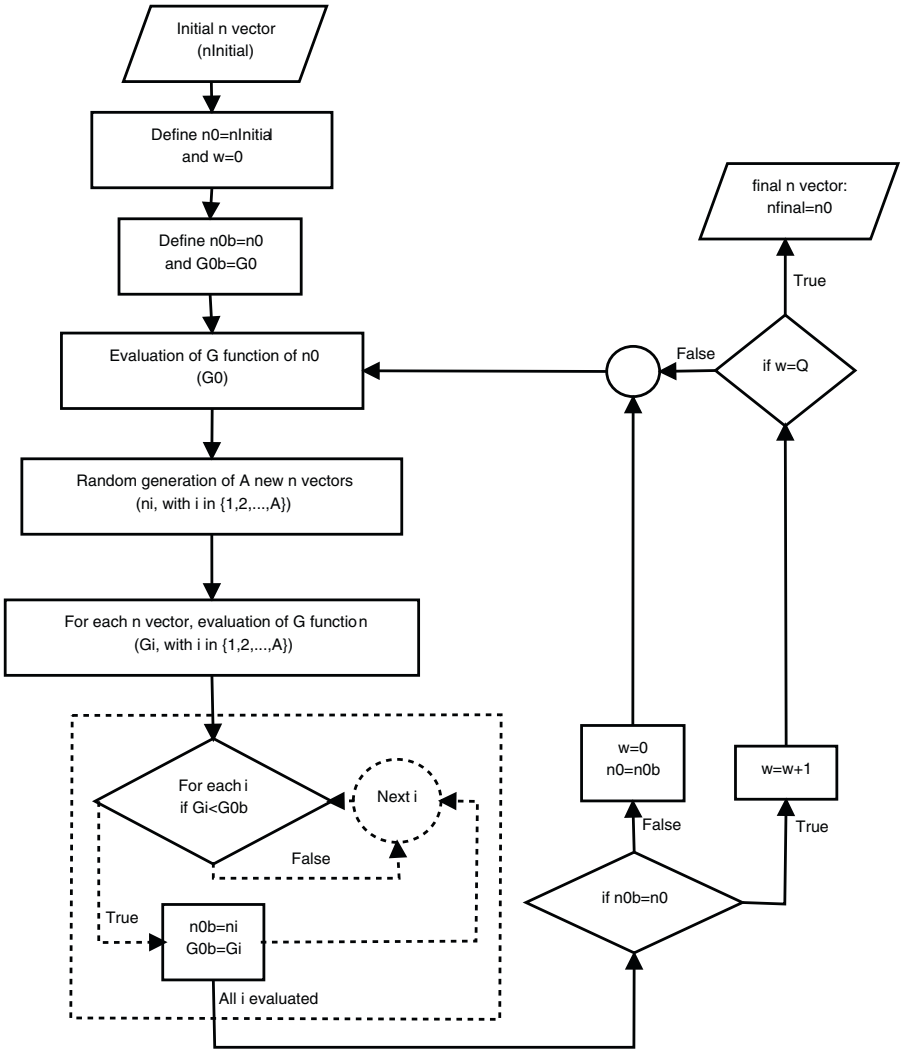

Fig. 2. Flow diagram for G function minimization routine. *A* (*ants*) is the number of random searches arround vector n0, set as 50; and *Q* is the maximum number of times the routine can cycle without establishing a new optimal value, set as 20. These values were set to ensure convergence.

bonaceous deposits should be formed, differing in morphology and reactivity [35,36]. An analysis conducted on a Ni catalyst showed 5 different types of carbon deposits, summarized in Table 1 [37]. This suggests that the use of graphite thermodynamic properties for carbonaceous deposits representation is incomplete. Thus this work aims to describe equilibrium composition for reforming systems, including carbon deposits properties besides graphite, improving the thermodynamic description of the carbonaceous species formation taking place at during ethanol reforming.

Table 1
Forms and reactivities of carbon species formed by decomposition of CO on nickel [37]. With permission of Elsevier [35].

Structure	Designation	Temperature of formation (°C)
Absorbed carbon atoms (dispersed, surface carbide)	C_α	200–400
Polymeric films and filaments (amorphous)	C_β	250–500
Vermicular filaments, fibers, and/or whiskers	C_V	300–1000
Nickel carbide (bulk)	C_γ	150–250
Graphitic platelets and films (crystalline)	C_c	500–550

2. Methodology

For predicting the equilibrium composition by Gibbs free energy minimization, the expression given by Eq. (6) has to be minimized [38], for a solid–gas system, under the assumption of ideal gases and excluding solids from the calculation of gas molar fraction.

$$G = \sum_{i=1}^{NC^g} n_i^g \left(\mu_i^{g,0} + RT \ln \left(\frac{n_i^g}{n_{\text{gases}}} \gamma_i P \right) \right) + \sum_{i=1}^{NC^s} n_i^s \mu_i^{s,0} \tag{6}$$

In Eq. (6), NC^g and NC^s are the number of components in gas and solid phase, respectively; n_i^g, the number of moles of component *i* in gas phase; n_i^s, the number of moles of component i in solid phase; *R*, the gas constant in [J/mol K]; *T*, the temperature in [K]; n_{gases}, the total number of moles in gas phase; *P*, adimensional pressure ($P_{\text{eval}}/P_{\text{std}}$); γ_i is the activity coefficient of component *i*; and $\mu_i^0 = \mu_i^0(T)$ is the chemical potential of species *i* at standard pressure, focusing on enthalpy information [39]. The chemical potential can be calculated from Eqs. (7)–(9) where $\underline{G_i}$ is the partial molar Gibbs free energy; $\underline{H_i}$, the partial molar enthalpy; and c_{p_i}, the heat capacity at constant pressure of component *i* [30,33,40].

$$\left(\frac{\partial \underline{H_i}}{\partial T} \right)_P = c_{p_i} \tag{7}$$

Table 2
Considered set of reactants and feasible products for ethanol reforming.

Gases		
Ethanol	Ethane	Diethyl ether
Oxygen	Ethylene	Ethylene glycol
Water	Acetylene	n-Propanol
Carbon dioxide	Acetaldehyde	iso-Propanol
Hydrogen	Acetic acid	n-Butanol
Carbon monoxide	Acetone	iso-Propyl-methyl-ether
Methane	Ethyl acetate	
Solids		
Graphite, C_C	Amorphous carbon deposits, C_β	Multi-wall carbon nanotubes (MWCNT), C_V

$$\frac{\partial}{\partial T}\left(\frac{\underline{G}_i}{RT}\right)_P = -\frac{\underline{H}_i}{RT^2} \tag{8}$$

$$\underline{G}_i = \mu_i \tag{9}$$

The considered component set are detailed in Table 2.

Eqs. (7)–(9) are solved directly for gases at standard pressure, obtaining:

$$\begin{aligned}\mu_i^0(T)\,[\mathrm{J/mol}] = {} & \left(\frac{T}{T_0}\right)\Delta G_{f_i}^0 + \left(1-\frac{T}{T_0}\right)\Delta H_{f_i}^0 \\ & - C1_i\left(T\ln\left(\frac{T}{T_0}\right) - T + T_0\right) - \frac{C2_i}{2}(T^2 - 2T_0T + T_0^2) \\ & - \frac{C3_i}{6}(T^3 - 3T_0^2T + 2T_0^3) - \frac{C4_i}{12}(T^4 - 4T_0^3T + 3T_0^4) \\ & - \frac{C5_i}{20}(T^5 - 5T_0^4T + 4T_0^5)\end{aligned} \tag{10}$$

$\Delta G_{f_i}^0$, $\Delta H_{f_i}^0$ and $C1_i$ to $C5_i$ (constants for polynomial expression of c_{p_i}) were taken from international databases [41,42].

For graphite, Eqs. (7)–(9) were solved by numerical integration, taking $c_{p_{\mathrm{graphite}}}$ from Eq. (11) [42].

$$c_{p_{\mathrm{graphite}}} = 4.184\left(2.673 + 0.002617T - \frac{116,900}{T^2}\right)\ [\mathrm{J/mol\,K}] \tag{11}$$

Since the data for MWCNT is not found in available databases, the chemical potential for this carbon specieswas calculated from

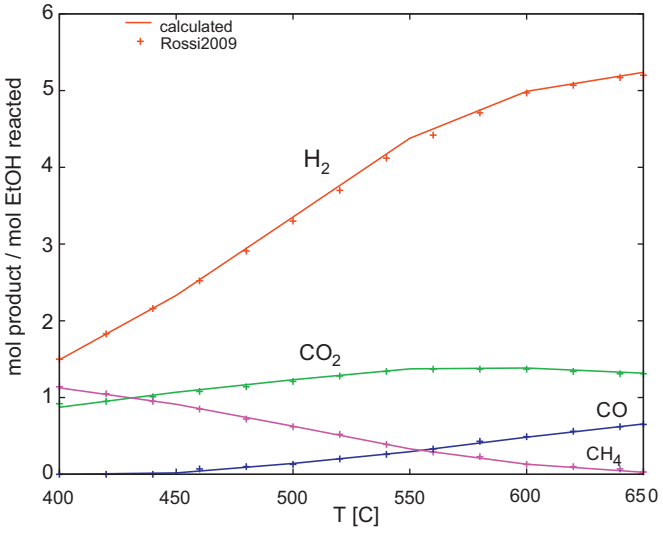

Fig. 3. Comparison of calculed equilibrium composition for SR of ethanol with Rossi et al. results [33].

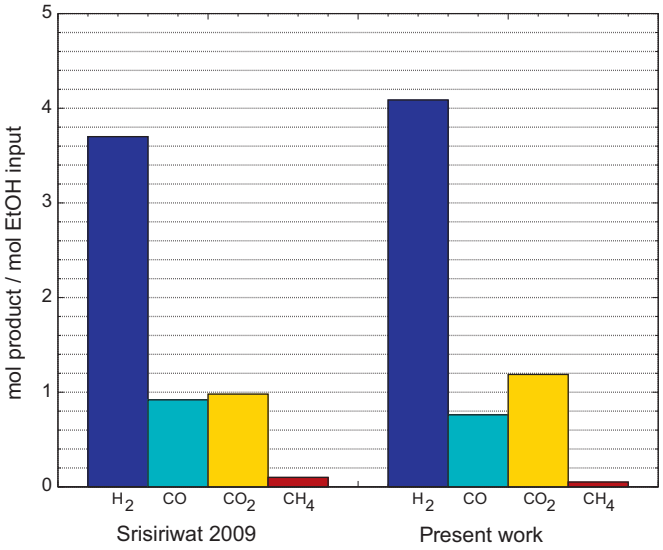

Fig. 4. Comparison between experimental data of Srisiriwat et al. [49] for OSR of ethanol on 15%$_{wt}$Ni/8%$_{wt}$$CeO_2$/$Al_2O_3$ catalyst and Gibbs free energy minimization routine for prediction of equilibrium composition exposed in Fig. 2. Reaction conditions were set as follow: S/E = 3, O/E = 0.26 and 700 °C.

Eq. (9), computing $\underline{G}_{\mathrm{MWCNT}}$ as a function of $\underline{G}_{\mathrm{graphite}}$ with the thermodynamic data for the reaction $C_{\mathrm{graphite}} \rightarrow C_{\mathrm{MWCNT}}$ [43]:

$$\begin{aligned}\underline{G}_{\mathrm{MWCNT}}\,[\mathrm{J/mol}] &= \underline{G}_{\mathrm{graphite}} + \Delta G^0_{\mathrm{graphite}\rightarrow\mathrm{MWCNT}} \\ &= \underline{G}_{\mathrm{graphite}} + 8250 - 11.72T\end{aligned} \tag{12}$$

For amorphous carbon deposits, $\underline{G}_{\mathrm{Amorphous\,carbon}}$ was computed by polynomial adjustment to thermodynamic data of pure carbon amorphous species [44,45]:

$$\begin{aligned}\underline{G}_{\mathrm{Amorphous\,carbon}}\,[\mathrm{J/mol}] = {} & -5.8239E - 12T^4 + 1.9769E - 8T^3 \\ & -2.7622E - 5T^2 + 9.8415E - 3T \\ & +1.4895E + 1 \\ R^2 = {} & 9.9944E - 1\end{aligned} \tag{13}$$

Eq. (6) was solved by an Ant algorithm [46,47] over a discrete type space. All composition vectors n (with 24 components max.)

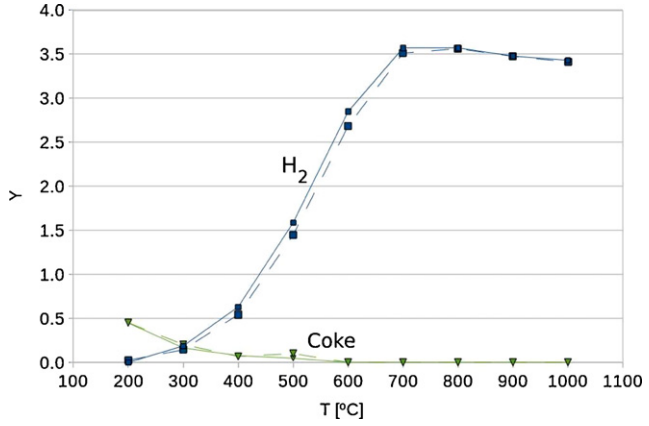

Fig. 5. Calculated yields for H_2 and carbon deposits supposed as graphite. MWCNT and amorphous carbon were removed from component set specified in Table 2 for replication of previous work [30]. O/E = 0.5, S/E = 2.0. (—) Rabenstein et al. data. (- - -) Data obtained with own algorithm.

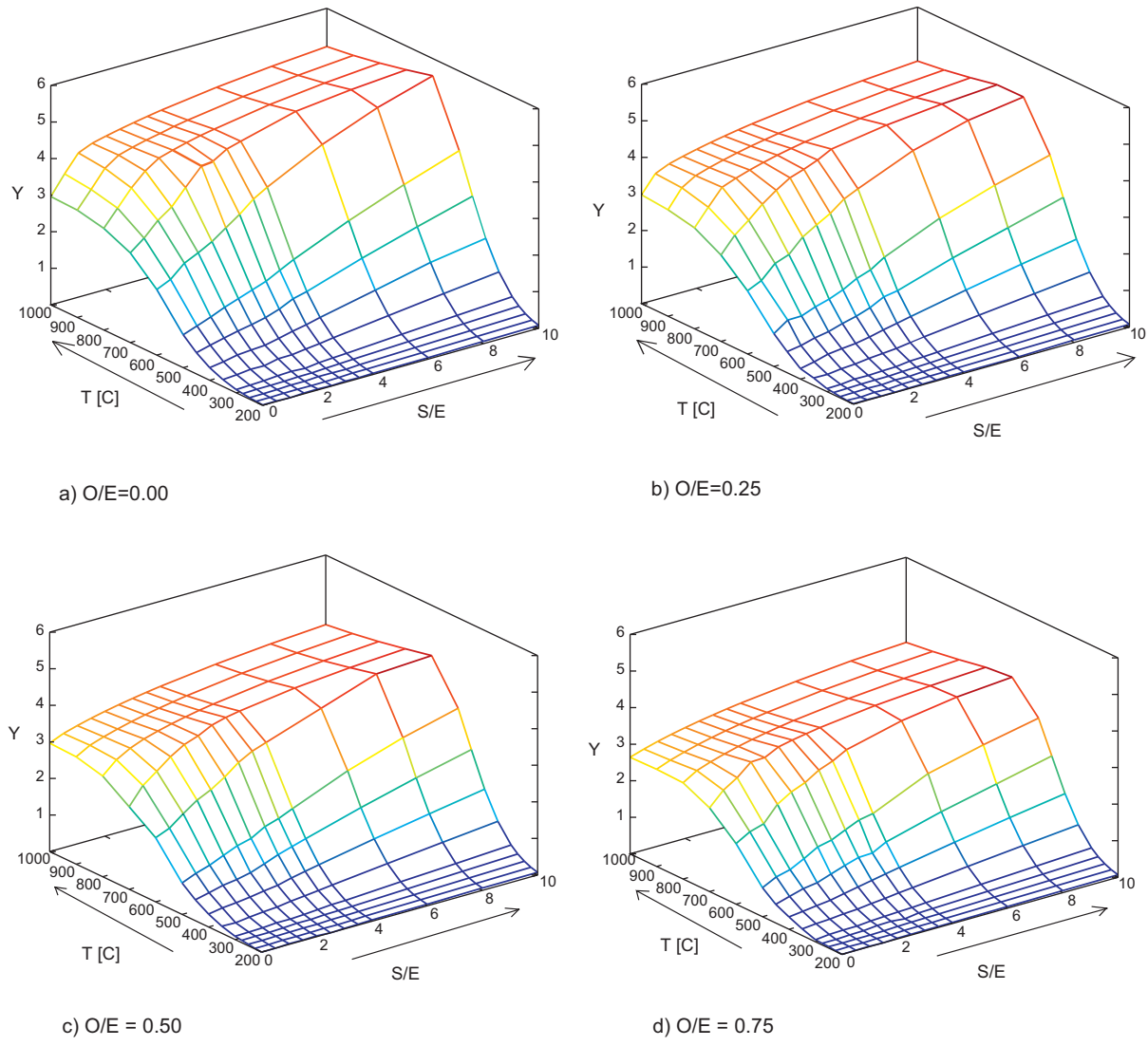

Fig. 6. Calculated yields for H_2 with different O/E ratio. All components in Table 2 were considered.

have constrains for their components, attending:

$$\text{Atom conservation}: \sum_i a_{ij} n_i = \sum_i^{NC} a_{ij} n_i^{\text{initial}};\ \forall j \in \{1, 2, \ldots, NA\} \tag{14}$$

$$\text{Non} - \text{negative molarity}: n_i \geq 0;\ \forall i \in \{1, 2, 3, \ldots, NC\} \tag{15}$$

n^{initial} is the initial composition vector; NA, the number of atoms in total composition; and a_{ij}, the number of j atoms in molecule i. The constrains exhibited in Eqs. (14) and (15) were incorporated on dimensional space by the construction method for composition vectors n. A simplified flow diagram of this construction routine is shown in Fig. 1.

As mentioned before, the search of the minimum of the G function (see Eq. (6)) was programmed emulating an Ant algorithm [46,47]. A flow diagram for minimization of function G is shown in Fig. 2.

All routines were implemented in GNU Octave numerical language [48]. Gibbs free energy minimization routine exhibited in Fig. 2 was used for predicting equilibrium composition of reforming systems.

3. Evaluation of the algorithm

The Gibbs free energy minimization routine allowed to estimate equilibrium composition of various systems. Fig. 3 shows a comparison of our results, considering partial set of components including ethanol, water, carbon dioxide, hydrogen, carbon monoxide, methane, ethane, ethylene, acetaldehyde and acetone, with those from the work of Rossi et al. [33]. The results obtained by our methodology are in good agreement with the theoretical data obtained by these authors, within the following proportional errors: 0.8% for H_2 yield; 1.2% for CO_2 yield; 2.2% for CO yield; and 5.3% for CH_4 yield. This confirms the algorithm used in this work was properly developed.

Experimental validation of a thermodynamic model is not always possible since the experimental data reported in literature is not necessarily at equilibrium conditions. Nonetheless it is still quite useful to compare experimental results with thermodynamics data to observe the trends and confirm how far apart is the system from equilibrium conditions. Fig. 4 shows a comparison between experimental work on OSR [49] and current thermodynamic calculations, revealing a close agreement and therefore indicating the proximity of Srisiriwat et al. experimental system to thermodynamic equilibrium.

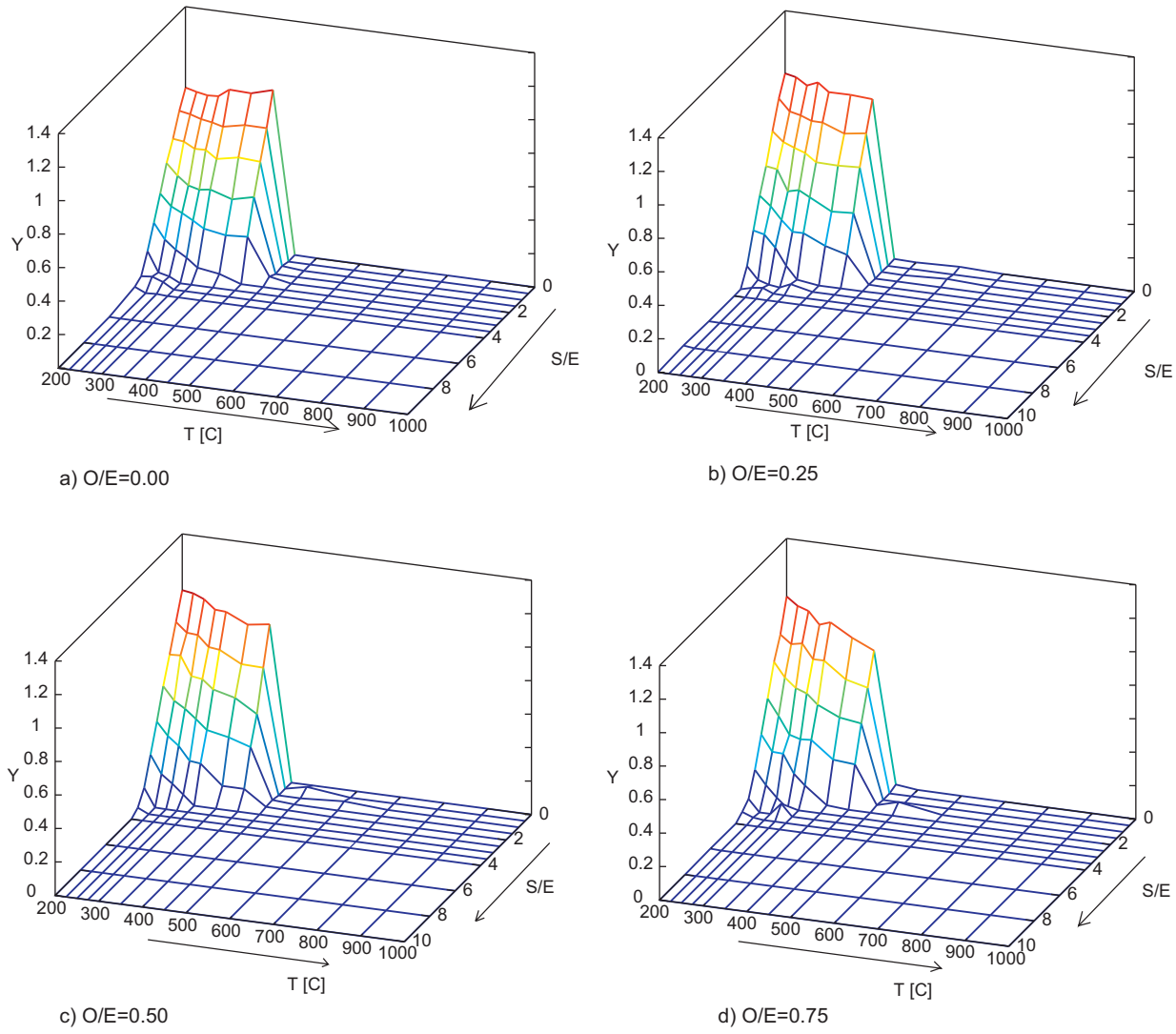

Fig. 7. Calculated yields for graphite with different O/E ratio. All components in Table 2 were considered.

As mentioned above, previous efforts related to the estimation of equilibrium output composition based on a thermodynamic analysis by Gibbs free energy minimization are concentrated in the gaseous species, and those who consider solid deposits formation, represent carbonaceous deposits simply as graphite [29–33]. Applying our routine to the component set specified in Table 2, but removing MWCNT and amorphous carbon, the calculation yields similar results as those of a previous work [30] (5). The results obtained by our routine are in good agreement with the theoretical data obtained by Rabenstein et al., within the following proportional errors: 1.7% for H_2 yield and 2.6% for coke yield.

The product yield (Y) is calculated as $mol_{product}/mol_{EtOH_{input}}$. These results indicate important formation of carbon deposits for low S/E ratios (below S/E = 3) at temperatures between 200 °C and 700 °C. This region corresponds also to the area of lowest hydrogen yield (Fig. 5).

4. Results and discussion

To extend these results the present study considered all components described in Table 2 and different O/E ratios. In such a way it is possible to analyze the formation of different carbonaceous species under OSR conditions. These results are shown in Figs. 6–8. No major changes are observed for the gaseous species at equilibrium after considering different types of carbon deposits. This result is showed for O/E = 0, 0.5 and S/E = 2, 4 in Fig. 9. Hydrogen yield slightly declines as O/E ratio increases, as shown in Fig. 6, due to the increase in the production of CO and H_2O under oxygen enriched conditions. Higher H_2 production is achieved at high temperatures (above 700 °C), high S/E ratio (>4) and low O/E ratio, as it has been showed for SR system versus POX or OSR systems [30].

The results shown in Figs. 7 and 8 confirm that the formation of carbonaceous species is favored at S/E ratios below 4.0 for all temperatures and O/E ratios. Nonetheless, our results indicate that the carbon species formed strongly depends on the temperature, showing a drastic change on the predominant carbon-containing species present at equilibrium.

Comparing equilibrium results for different carbon species, in Figs. 7 and 8, is possible to note that below 400 °C there is mainly formation of graphite carbon, and for higher temperatures and below a S/E ratio of 3, the graphite carbon species completely disappears to give rise to MWCNT structures that remains present even at temperatures as high as 1000 °C for S/E and O/E equal to 0. This behavior, strongly related to temperature changes, is consistent with reports indicating that higher temperature promotes carbon nanotubes formation [37].

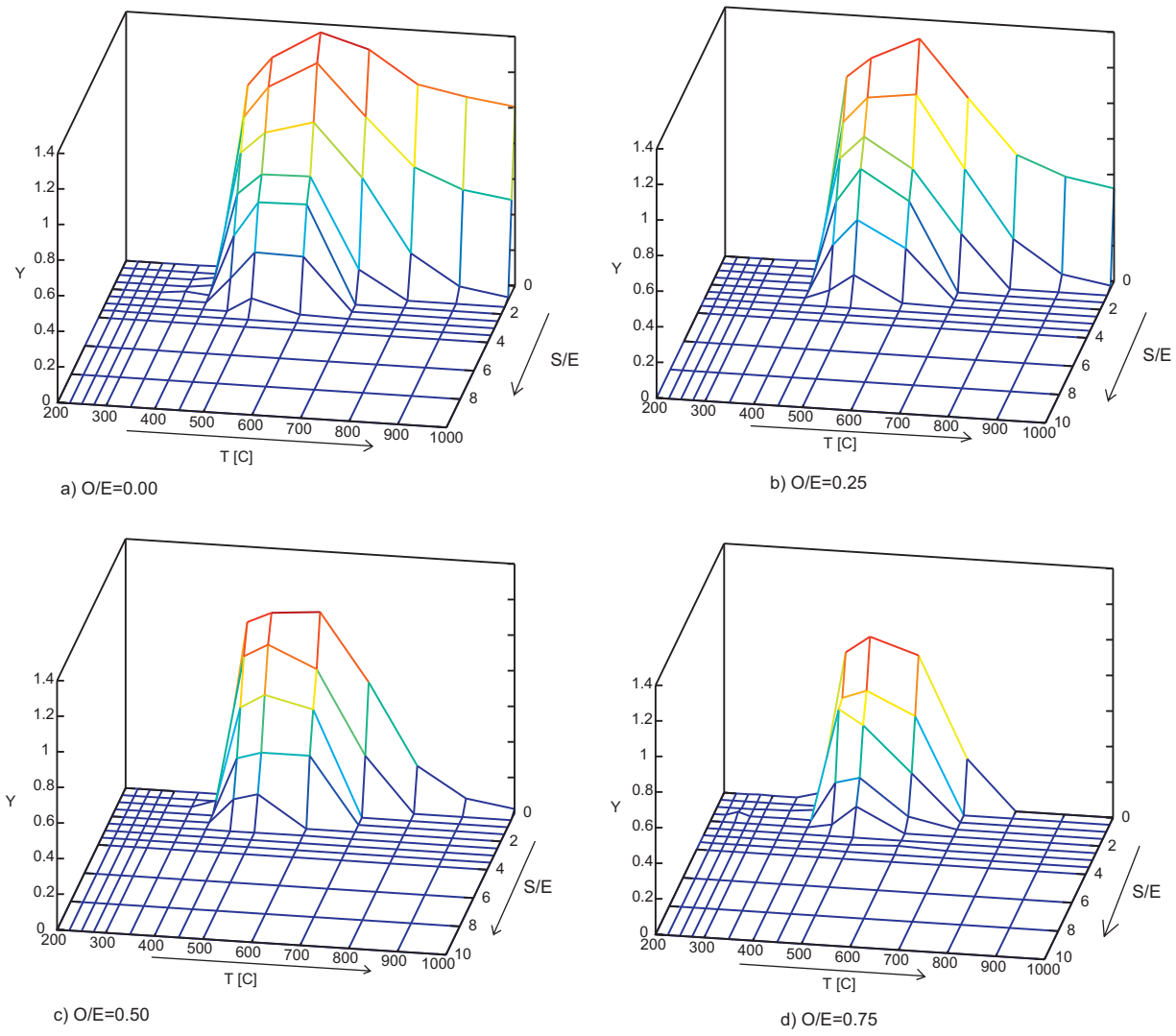

Fig. 8. Calculated yields for MWCNT with different O/E ratio. All components in Table 2 were considered.

The change of the predominant carbonaceous species is also clear in Fig. 10. This figure compares the total amount of carbon deposits when only the graphite species is considered (solid line) and the case when amorphous carbon, graphite, and MWCNT species are considered (broken line). It is clear that the total carbon amount is higher when a multiple representation is used, mainly due to the inclusion of MWCNT in the component set. Again, MWCNT formation is higher than graphite species at temperatures above 400 °C, that coincides with the temperature range where the larger differences in the amount of carbon species is observed. As the O/E ratio grows, less MWCNT is formed, but the difference in the total amount of carbon formed still remains.

Another important observation is that the disappearance of MWCNT species is faster at higher temperatures, especially above 700 °C, which agrees with real systems observations, were O_2 presence promotes combustion of coke [34]. In contrast, this behavior is not observed in graphite equilibrium calculations (Fig. 7).

It must be noted that the disappearance of the carbon-containing species with O/E ratio increment have been reported in previous equilibrium calculations [30], but considering all solid carbonaceous species as graphite. Our results indicate that the change in deposits formation with O/E ratio is mainly due to carbon nanotubes disappearance (Fig. 8) instead of graphite (Fig. 7), which yield remains almost constant even under variations of the O/E ratio to oxygen-rich conditions.

High S/E ratio also prevents carbonaceous species formation, which effect is evidenced in Fig. 10. Equilibrium results indicate that, at S/E ratio of 4 or higher, both graphite and MWCNT formation is inhibited as seen in Figs. 7 and 8.

According to these results, there is no presence of amorphous carbon at equilibrium conditions. However, there are several reports in real systems showing amorphous carbon deposits, whose crystal structure is less orderly than that of graphite or MWCNT [50–52]. The absence of amorphous carbon at equilibrium conditions may indicate a faster formation kinetics for amorphous carbon than for graphite or MWCNT, justifying the existence of amorphous carbon in real experimental systems controlled by kinetic aspect. Another possible explanation is that its formation is not properly described by just considering pure C species. Further work is underway to incorporate additional information on the carbon nanotubes formation, considering different diameters and lengths, as well as to improve the Gibbs free energy calculation for amorphous carbon.

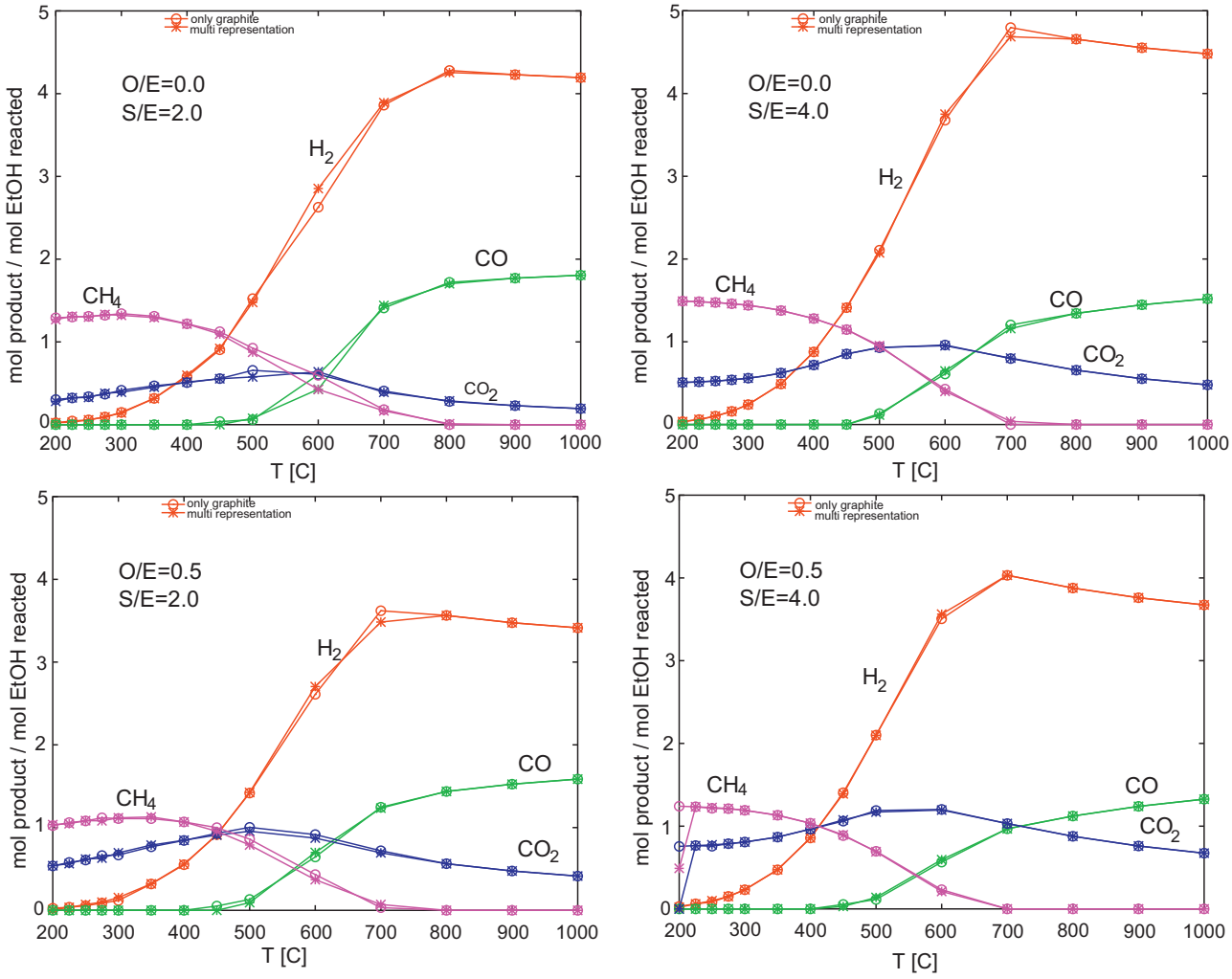

Fig. 9. Gas equilibrium composition for O/E = 0.0, 0.5 and S/E = 2, 4 when only graphite (◯) or graphite, MWCNT and amorphous carbon (*) where considered in carbonaceous deposits representation.

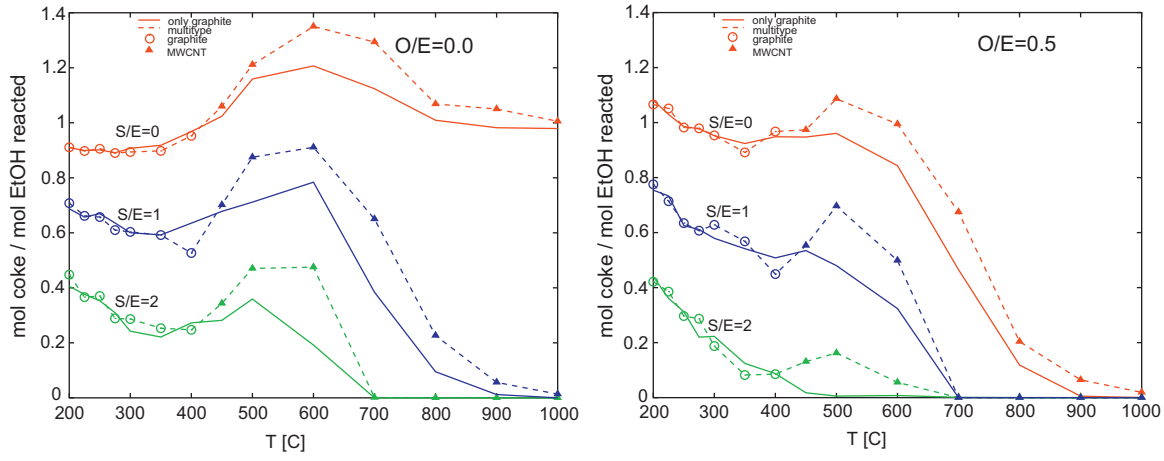

Fig. 10. Total amount of carbon deposits for O/E = 0 and O/E = 0.5 when only graphite (solid line) or graphite, MWCNT, and amorphous carbon were considered in carbonaceous deposits representation (broken line). The (◯) symbols represent graphite deposits; and the (▲) symbols, MWCNT deposits, illustrating the main carbon deposits distribution.

5. Conclusions

This work presents the study of thermodynamical equilibrium composition for different reforming systems, including the description of carbon deposits other than graphite carbon. The inclusion of MWCNT and amorphous carbon reveals the existence of well defined regions with clear temperature and S/E ratio limits.

In equilibrium, carbon deposits are formed when S/E ratio is below 4. In this zone, temperature defines which carbon type is formed: below 400 °C the presence of graphite domines, while above 400 °C prevails MWCNT.

According to our results, the disappearance of carbon deposits as the O/E ratio increasesis mainly due to the removal of MWCNT species rather than the graphitic species.

No amorphous carbon is obtained in equilibrium, so better thermodynamic representation is being developed to represent its presence in real systems.

Acknowledgments

The funding from Fondecyt project No. 1090232, and CONICYT Doctoral Fellowship (F. Díaz Alvarado) are gratefully acknowledged.

References

[1] E. Örücü, M. Karakaya, A.K. Avcl, Z.I. Önsan, Investigation of ethanol conversion for hydrogen fuel cells using computer simulations, Journal of Chemical Technology and Biotechnology 80 (10) (2005) 1103–1110.
[2] A. Fatsikostas, D. Kondarides, X. Verykios, Production of hydrogen for fuel cells by reformation of biomass-derived ethanol, Catalysis Today 75 (1–4) (2002) 145–155.
[3] P.D. Vaidya, A.E. Rodrigues, Insight into steam reforming of ethanol to produce hydrogen for fuel cells, Chemical Engineering Journal 117 (1) (2006) 39–49.
[4] A. Haryanto, S. Fernando, N. Murali, S. Adhikari, Current status of hydrogen production techniques by steam reforming of ethanol: a review, Energy and Fuels 19 (5) (2005) 2098–2106.
[5] Z.I. Önsan, Catalytic processes for clean hydrogen production from hydrocarbons, Turkish Journal of Chemistry 31 (2007) 531–550.
[6] D.L. Trimm, Z.I. Önsan, Onboard fuel conversion for hydrogen-fuel-cell-driven vehicles, Catalysis Reviews 43 (1) (2001) 31–84.
[7] A.E. Farrell, R.J. Plevin, B.T. Turner, A.D. Jones, M. O'Hare, D.M. Kammen, Ethanol can contribute to energy and environmental goals, Science 311 (5760) (2006) 506–508.
[8] M. Wang, C. Saricks, D. Santini, Effects of fuel ethanol use on fuel-cycle energy and greenhouse gas emissions, Tech. rep., Argonne National Laboratory, USDOE, 2006.
[9] M. Wu, M. Wang, H. Huo, Fuel-cycle assessment of selected bioethanol production pathways in the united states, Tech. rep., Argonne National Laboratory, USDOE, 2006.
[10] S. Cavallaro, Ethanol steam reforming on rh/al2o3 catalysts, Energy and Fuels 14 (6) (2000) 1195–1199.
[11] M. Ni, D.Y. Leung, M.K. Leung, A review on reforming bio-ethanol for hydrogen production, International Journal of Hydrogen Energy 32 (15) (2007) 3238–3247.
[12] R. Navarro, M. Ãlvarez Galván, M.C. Sánchez-Sánchez, F. Rosa, J. Fierro, Production of hydrogen by oxidative reforming of ethanol over pt catalysts supported on al2o3 modified with ce and la, Applied Catalysis B: Environmental 55 (4) (2005) 229–241.
[13] NIST, NIST Chemistry WebBook, The National Institute of Standards and Technology, U.S. Secretary of Commerce, 2005.
[14] S.M. de Lima, I.O. da Cruz, G. Jacobs, B.H. Davis, L.V. Mattos, F.B. Noronha, Steam reforming, partial oxidation, and oxidative steam reforming of ethanol over pt/cezro2 catalyst, Journal of Catalysis 257 (2) (2008) 356–368.
[15] G.A. Deluga, J.R. Salge, L.D. Schmidt, X.E. Verykios, Renewable hydrogen from ethanol by autothermal reforming, Science 303 (5660) (2004) 993–997.
[16] H.-S. Roh, A. Platon, Y. Wang, D.L. King, Catalyst deactivation and regeneration in low temperature ethanol steam reforming with rh/ceo2zro2 catalysts, Catalysis Letters 110 (1/2) (2006) 1–6.
[17] J. Comas, F. Mariño, M. Laborde, N. Amadeo, Bio-ethanol steam reforming on ni/al2o3 catalyst, Chemical Engineering Journal 98 (1–2) (2004) 61–68.
[18] J. Sun, X.-P. Qiu, F. Wu, W.-T. Zhu, H2 from steam reforming of ethanol at low temperature over ni/y2o3, ni/la2o3 and ni/al2o3 catalysts for fuel-cell application, International Journal of Hydrogen Energy 30 (4) (2005) 437–445.
[19] A. Erdöhelyi, J. Raskö, T. Kecskés, M. Tóth, M. Dömök, K. Baán, Hydrogen formation in ethanol reforming on supported noble metal catalysts, Catalysis Today 116 (3) (2006) 367–376.
[20] F. Frusteri, S. Freni, V. Chiodo, S. Donato, G. Bonura, S. Cavallaro, Steam and autothermal reforming of bio-ethanol over mgo and ceo2 ni supported catalysts, International Journal of Hydrogen Energy 31 (15) (2006) 2193–2199.
[21] P. Vaidya, A. Rodrigues, Kinetics of steam reforming of ethanol over a ru/al2o3 catalyst, Industrial and Engineering Chemistry Research 45 (19) (2006) 6614–6618.
[22] H. Song, L. Zhang, R.B. Watson, D. Braden, U.S. Ozkan, Investigation of bio-ethanol steam reforming over cobalt-based catalysts, Catalysis Today 129 (3–4) (2007) 346–354.
[23] J. Liberatori, R. Ribeiro, D. Zanchet, F. Noronha, J. Bueno, Steam reforming of ethanol on supported nickel catalysts, Applied Catalysis A: General 327 (2) (2007) 197–204.
[24] F. Soyal-Baltacloglu, A.E. Aksoylu, Z.I. Önsan, Steam reforming of ethanol over pt-ni catalysts, Catalysis Today 138 (3–4) (2008) 183–186.
[25] E.B. Pereira, N. Homs, S. Marti, J. Fierro, P. Ramirez de la Piscina, Oxidative steam-reforming of ethanol over co/sio2, co-rh/sio2 and co-ru/sio2 catalysts: catalytic behavior and deactivation/regeneration processes, Journal of Catalysis 257 (1) (2008) 206–214.
[26] W. Cai, F. Wang, A. Van Veen, H. Provendier, C. Mirodatos, W. Shen, Autothermal reforming of ethanol for hydrogen production over an rh/ceo2 catalyst, Catalysis Today 138 (3–4) (2008) 152–156.
[27] M. Virginie, M. Araque, A.-C. Roger, J.C. Vargas, A. Kiennemann, Comparative study of h2 production by ethanol steam reforming on ce2zr1.5co0.5o8-[delta] and ce2zr1.5co0.47rh0.07o8-[delta]: evidence of the rh role on the deactivation process, Catalysis Today 138 (1–2) (2008) 21–27.
[28] A. Aguayo, A. Gayubo, A. Atutxa, M. Olazar, J. Bilbao, Catalyst deactivation by coke in the transformation of aqueous ethanol into hydrocarbons. Kinetic modeling and acidity deterioration of the catalyst, Industrial and Engineering Chemistry Research 41 (17) (2002) 4216–4224.
[29] S. Liu, K. Zhang, L. Fang, Y. Li, Thermodynamic analysis of hydrogen production from oxidative steam reforming of ethanol, Energy and Fuels 22 (2) (2008) 1365–1370.
[30] G. Rabenstein, V. Hacker, Hydrogen for fuel cells from ethanol by steam-reforming, partial-oxidation and combined auto-thermal reforming: a thermodynamic analysis, Journal of Power Sources 185 (2) (2008) 1293–1304.
[31] W. Wang, Y. Wang, Thermodynamic analysis of steam reforming of ethanol for hydrogen generation, International Journal of Energy Research 32 (15) (2008) 1432–1443.
[32] W. Wang, Y. Wang, Thermodynamic analysis of hydrogen production via partial oxidation of ethanol, International Journal of Hydrogen Energy 33 (19) (2008) 5035–5044.
[33] C. Rossi, C. Alonso, O. Antunes, R. Guirardello, L. Cardozo-Filho, Thermodynamic analysis of steam reforming of ethanol and glycerine for hydrogen production, International Journal of Hydrogen Energy 34 (1) (2009) 323–332.
[34] S. Cavallaro, V. Chiodo, S. Freni, N. Mondello, F. Frusteri, Performance of rh/al2o3 catalyst in the steam reforming of ethanol: H_2 production for mcfc, Applied Catalysis A: General 249 (1) (2003) 119–128.
[35] C.H. Bartholomew, Mechanisms of catalyst deactivation, Applied Catalysis A: General 212 (1–2) (2001) 17–60.
[36] J.M. Ginsburg, J. Piña, T. El Solh, H.I. de Lasa, Coke formation over a nickel catalyst under methane dry reforming conditions: Thermodynamic and kinetic models, Industrial and Engineering Chemistry Research 44 (14) (2005) 4846–4854.
[37] C.H. Bartholomew, Carbon deposition in steam reforming and methanation, Catalysis Reviews, Science and Engineering 24 (1982) 67–112.
[38] J. Castillo, I. Grossmann, Computation of phase and chemical equilibria, Computers and Chemical Engineering 5 (1981) 99–108.
[39] C. Rossi, L. Cardozo-Filho, R. Guirardello, Gibbs free energy minimization for the calculation of chemical and phase equilibrium using linear programming, Fluid Phase Equilibria 278 (1–2) (2009) 117–128.
[40] H.C. VanNess, M.M. Abbott, Perry's Chemical Engineers' Handbook, 7th ed., McGraw-Hill Companies, Inc., 1999 (Ch. Thermodynamics, pp. 4.1–4.36).
[41] CHERIC, Korea Thermophysical Properties Data Bank, Chemical Engineering Research Information Center, 2009.
[42] P.E. Liley, G.H. Thomson, D.G. Friend, T.E. Daubert, E. Buck, Perry's Chemical Engineers' Handbook, 7th ed., McGraw-Hill Companies, Inc., 1999 (Ch. Physical and Chemical Data, pp. 2.1–2.374).
[43] D. Gozzi, M. Iervolino, A. Latini, The thermodynamics of the transformation of graphite to multiwalled carbon nanotubes, Journal of the American Chemical Society 129 (33) (2007) 10269–10275.
[44] R.O. Outokumpu, HSC Chemistry 5.1, Outokumpu Research Oy, Finland, 2002.
[45] M. Karapet'yants, M. Karapet'yants, Thermodynamic Constants of Inorganic and Organic Compounds, Ann Arbor-Humphrey, London, 1970.
[46] M. Dorigo, G. Di Caro, L.M. Gambardella, Ant algorithms for discrete optimization, Artificial Life 5 (2) (1999) 137–172.
[47] R. Mullen, D. Monekosso, S. Barman, P. Remagnino, A review of ant algorithms, Expert Systems with Applications 36 (6) (2009) 9608–9617.
[48] J.W. Eaton, Gnu octave, version 3.2.0, University of Wisconsin, Department of Chemical Engineering, 2009.
[49] N. Srisiriwat, S. Therdthianwong, A. Therdthianwong, Oxidative steam reforming of ethanol over ni/al2o3 catalysts promoted by ceo2, zro2 and ceo2-zro2, International Journal of Hydrogen Energy 34 (5) (2009) 2224–2234.
[50] H. Wang, Y. Liu, L. Wang, Y. Qin, Study on the carbon deposition in steam reforming of ethanol over co/ceo2 catalyst, Chemical Engineering Journal 145 (1) (2008) 25–31.
[51] H. Song, U.S. Ozkan, Ethanol steam reforming over co-based catalysts: role of oxygen mobility, Journal of Catalysis 261 (1) (2009) 66–74.
[52] S. Osswald, M. Havel, Y. Gogotsi, Monitoring oxidation of multiwalled carbon nanotubes by raman spectroscopy, Journal of Raman Spectroscopy 38 (6) (2007) 728–736.